INSTITUTE OF PHYSICS PUBLISHING JOURNAL OF PHYSICS A: MATHEMATICAL AND GENERAL

J. Phys. A: Math. Gen. **36** (2003) 11037–11053 PII: S0305-4470(03)64830-4

Bicolouring random hypergraphs

Tommaso Castellani[1], **Vincenzo Napolano**[2], **Federico Ricci-Tersenghi**[1] **and Riccardo Zecchina**[3]

[1] Dipartimento di Fisica, SMC and INFM, Università di Roma 'La Sapienza', Piazzale Aldo Moro 2, I-00185 Roma, Italy
[2] Dipartimento di Fisica, Università di Trieste, Via Valerio 2, I-34127 Trieste, Italy
[3] International Center for Theoretical Physics, Strada Costiera 11, PO Box 586, I-34100 Trieste, Italy

Received 16 June 2003, in final form 28 July 2003
Published 15 October 2003
Online at stacks.iop.org/JPhysA/36/11037

Abstract

We study the problem of bicolouring random hypergraphs, both numerically and analytically. We apply the zero-temperature cavity method to find analytical results for the phase transitions (dynamic and static) in the one-step replica symmetry breaking (1RSB) approximation. These points appear to be in agreement with the results of the numerical algorithm. In the second part, we implement and test the survey propagation algorithm for specific bicolouring instances in the so-called HARD-SAT phase.

PACS numbers: 89.20.Ff, 75.10.Nr, 05.70.Fh

1. Introduction

The hypergraph bicolouring is one of the classic combinatorial optimization problems belonging to the NP-complete class [1]. Its random version, bicolouring of random hypergraphs, is a very interesting problem for the phase transitions it shows. Indeed, varying the average connectivity of the random hypergraph, the model undergoes a transition [2] from a phase in which all links can be properly coloured to a phase in which a sizable fraction of links are violated. Around the transition point most difficult instances accumulate.

A graph is an ensemble of sites and links between them. In a hypergraph, the links connect triplets of sites. Each site (or vertex) can be coloured in two ways, say black or white, so it is natural to identify it with an Ising spin variable that can assume the value 1 or -1. The link is considered to be satisfied if the three spins that share it are not all of the same colour. In the following we will often refer to a link as a function node, as it is called, for example, in the K-SAT problem [3]. The bicolouring problem consists in finding an assignment to all spins such that all the links are satisfied. Consequently, a graph will be called colourable or uncolourable.

We can write the Hamiltonian for the problem assuming that each unsatisfied link gives a positive energy and zero otherwise. The total energy is proportional to the number of

unsatisfied links: a colourable hypergraph will have a zero-energy ground state, while a non-colourable one will have a positive-energy ground state.

The Hamiltonian for bicolouring a hypergraph $\mathcal{G}$ reads

$$\mathcal{H} = \sum_{\{i,j,k\}\in\mathcal{G}} \frac{1+\sigma_i\sigma_j+\sigma_i\sigma_k+\sigma_j\sigma_k}{2} \tag{1}$$

where $\sigma_i = \pm 1$ are Ising variables (corresponding to the two available colours) and the sum runs over all the hyperedges of $\mathcal{G}$. Note that a factor of 2 has been introduced for computational convenience[4].

Each term in the above sum is equal to 2 if and only if all the spins in the same interaction are parallel, that is if all the vertices connected by a hyperedge have the same colour. The Hamiltonian in equation (1) thus counts twice the number of badly coloured hyperedges. Perfect colourations correspond to zero-energy configurations.

In the present work we focus on colourability of random hypergraphs with N vertices and M hyperedges, varying the relevant parameter $\alpha = \frac{M}{N}$. In a typical random hypergraph the connectivity of a spin (i.e. the degree of a vertex) is a random variable distributed according to a Poissonian of mean 3α.

Analogous to random K-SAT [3], random K-XORSAT [4] and Q-colouring of random graphs [5], the random hypergraph bicolouring is expected to undergo two phase transitions increasing α. The first one is called 'dynamical transition' and is located at α_d where solutions to the problem (perfect colourations) undergo a clustering phenomenon. At this point the complexity Σ, which counts the number of clusters of solutions, becomes nonzero. We recall that if $\mathcal{N}(E)$ is the number of states at energy E the complexity is defined by the relation $\mathcal{N}(E) = \exp N\Sigma(\alpha, E/N)$, and so it is a function of α and the energy density. In the region where the complexity becomes positive, on top of a large number of ground states there appear an even larger number of metastable states: the latter may trap and slow down linear-time colouring algorithms and local search randomized methods [6]. At present all known linear-time colouring algorithms stop converging for α values well below α_d.

The second transition takes place at α_c, where the ground-state energy becomes positive: for $\alpha < \alpha_c$ most of the hypergraphs are colourable, while for $\alpha > \alpha_c$ most of them are not. This transition is formally equivalent to the so-called SAT/UNSAT transition of K-SAT [3, 7] and K-XORSAT [4], and we will refer to it with this name, although it is also known as 'COL/UNCOL' transition in the computer science literature.

Known results on the SAT/UNSAT transition are only upper and lower bounds. The best upper bound for α_c, found with rigorous calculation, is 2.409 [8]. The best lower bound is 3/2 [9]. In [10] the more general problem of bicolouring random hypergraphs with p-spin hyperlinks is analysed. However for the $p = 3$ case the bounds are worse than those we mentioned above. Recent rigorous results on random spin models and random K-SAT (K even) [11, 12] have shown that the one-step replica symmetry breaking (1RSB) results provide rigorous upper bounds to the phase transition point and we expect the same to be true in our case.

2. Numerical results

We wrote a recursive Davis–Putnam algorithm [13] to colour random finite-size hypergraph in order to localize the point α_c, which will be calculated analytically in the next sections. Here we present the numerical results, whose uncertainties are very small, thanks to the average of a large number of disorder realizations. In figure 1 (left) we show that the energy curves

[4] Local fields will turn out to be integer valued rather than fractional.

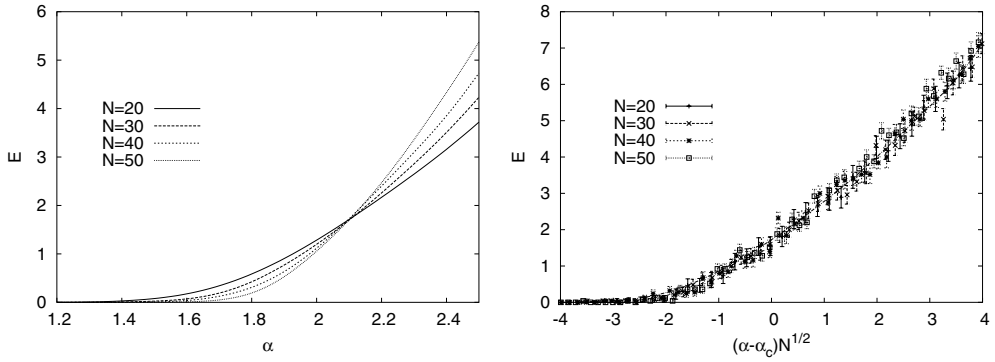

Figure 1. Left: average extensive energy for sizes $N = 20, 30, 40, 50$. The crossing point roughly localizes the SAT/UNSAT transition. Right: average extensive energy as a function of the rescaled variable $(\alpha - \alpha_c)N^{1/2}$. Data are represented with standard deviations.

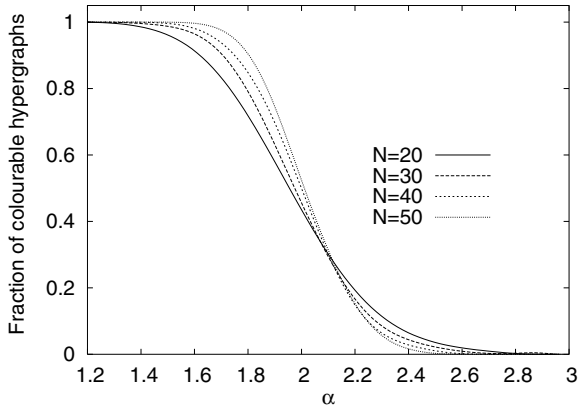

Figure 2. Fraction of colourable hypergraphs at $N = 20, 30, 40, 50$. The finite-size corrections are in this case larger and the crossing point is less clearly localized.

for different N cross at α_c. Indeed for $\alpha < \alpha_c$, $\lim_{N\to\infty} E = 0$ because all hypergraphs are colourable, while for $\alpha > \alpha_c$, $E \propto N$ and diverges for $N \to \infty$. From figure 1 we estimate $\alpha_c \simeq 2.1$. All the curves can be nicely collapsed when plotted versus $(\alpha - \alpha_c)N^{1/2}$, see figure 1 (right).

A second estimate of α_c can be obtained from the curves of the probability of being colourable as a function of α (see figure 2). However, here the crossing point is less clear because of larger finite-size corrections.

3. The cavity replica symmetric solution

3.1. Self-consistency equations

We now study the bicolouring problem with the cavity method at zero temperature [14, 15]. The simplest form of the zero-temperature cavity method is the replica symmetric (RS) approximation, in which we suppose the system to have a single state. The basic hypothesis of the cavity method is the lack of correlation between two randomly chosen spins, because of

the local tree structure of the hypergraph. Thanks to these vanishing correlations, the energy of the system for fixed σ_0 can be written as a function of the cavity fields h_j and g_j on the $2k$ neighbours of σ_0 [15]:

$$E(\sigma_0) = E_0 - \sum_{j=1}^{k} \hat{w}(g_j, h_j) - \sigma_0 \sum_{j=1}^{k} \hat{u}(g_j, h_j). \tag{2}$$

In the case of hypergraph bicolouring the functions $\hat{u}$ and $\hat{w}$ are given by

$$\begin{cases} \hat{u}(h_2, h_3) = \theta(-h_2)\theta(-h_3) - \theta(h_2)\theta(h_3) \\ \hat{w}(h_2, h_3) = |h_2| + |h_3| - |u(h_2, h_3)| \end{cases} \tag{3}$$

where $\theta(x) = 1$ if $x > 0$ and $\theta(x) = 0$ otherwise. The $\hat{u}$ are integers and can assume the value 0, 1 or -1. Note that $\hat{w} = \sum |h| - |u|$ is a general relation for models with Ising-type variables.

In the thermodynamic limit, we can assume the probability distributions of cavity fields h and cavity biases u to have well-defined limits, and write for them self-consistency equations:

$$\begin{cases} Q(u) = \int \mathrm{d}P(h_1)\,\mathrm{d}P(h_2)\delta(u - \hat{u}(h_1, h_2)) \\ P(h) = \sum_{k=0}^{\infty} f_{3\alpha}(k) \int \mathrm{d}Q(u_1) \cdots \mathrm{d}Q(u_k)\delta\big(h - \sum_{i=1}^{k} u_i\big) \end{cases} \tag{4}$$

with

$$f_{3\alpha}(k) = \frac{(3\alpha)^k}{k!}\,\mathrm{e}^{-3\alpha}.$$

As expected, these equations coincide with those obtained from a replica calculation in [16].

Exploiting system symmetries one can always write

$$Q(u) = c_0\delta(u) + \frac{1 - c_0}{2}[\delta(u + 1) + \delta(u - 1)]. \tag{5}$$

Analogously, the distribution of cavity fields can be written as $P(h) = \sum_{i=-\infty}^{\infty} p_i\delta(h - i)$, where the coefficients p_i are symmetric, i.e. $p_i = p_{-i}$. The self-consistency equations can then be written in terms of p_0 and c_0 as

$$\begin{cases} p_0 = \mathrm{e}^{-3\alpha(1-c_0)} I_0(3\alpha(1 - c_0)) \\ c_0 = 1 - \frac{(1-p_0)^2}{2} \end{cases} \tag{6}$$

where $I_0(x)$ is the zero-order modified Bessel function. c_0 is the order parameter of the system and it satisfies the self-consistency equation

$$1 - \sqrt{2(1 - c_0)} = \mathrm{e}^{-3\alpha(1-c_0)} I_0(3\alpha(1 - c_0)). \tag{7}$$

For any α value a 'paramagnetic' solution $c_0 = 1$ exists, for which all the cavity fields are zero. For $\alpha > \alpha_{\mathrm{RS}} = 2.3336$, there also exists a non-trivial 'glassy' solution with $c_0 < 1$.

3.2. Energy density

We now compute the RS energy density, following the notation already used in [15]. We must compute $E(\alpha) = \Delta E_1 - 2\alpha\Delta E_3$ where

$$\begin{aligned} \Delta E_3 = \int \mathrm{d}P(h_1)\,\mathrm{d}P(h_2)\,\mathrm{d}P(h_3) \Bigg[\min_{\sigma_1,\sigma_2,\sigma_3} \Bigg(\frac{1 + \sigma_1\sigma_2 + \sigma_2\sigma_3 + \sigma_1\sigma_3}{2} \\ - h_1\sigma_1 - h_2\sigma_2 - h_3\sigma_3 \Bigg) + |h_1| + |h_2| + |h_3|) \Bigg] \\ = 2 \int \mathrm{d}P(h_1)\,\mathrm{d}P(h_2)\,\mathrm{d}P(h_3)\,\theta(h_1h_2)\theta(h_2h_3) = \frac{1}{2}(1 - p_0)^3 = \sqrt{2}(1 - c_0)^{\frac{3}{2}} \end{aligned} \tag{8}$$

$$\Delta E_1 = \sum_{k=0}^{\infty} f_{3\alpha}(k) \int \mathrm{d}Q(u_1)\cdots\mathrm{d}Q(u_k) \left(\sum_{i=1}^{k} |u_i| - \left| \sum_{i=1}^{k} u_i \right| \right)$$

$$= 3\alpha(1-c_0) - 2\,\mathrm{e}^{-3\alpha(1-c_0)} \sum_{r=1}^{\infty} r I_r(3\alpha(1-c_0)). \tag{9}$$

If we introduce the parameter $\lambda = 3\alpha(1-c_0)$ which satisfies the equivalent of equation (7), the total RS energy density can be written as follows:

$$E = \lambda - 2\,\mathrm{e}^{-\lambda} \sum_{r} r I_r(\lambda) - \frac{2}{3}\lambda(1 - \mathrm{e}^{-\lambda} I_0(\lambda)). \tag{10}$$

Expression (10) seems to be the same for the different models with Ising variables (such as p-spin [17], K-SAT [18], etc), the difference being only in the self-consistency equation for λ, where α is multiplied by a different constant. For example, the α_{RS} value for the present bicolouring model is twice the value it takes in the three-spin model [17].

3.3. RS phase diagram

If we plot the energy (10) versus α we see that the energy of the non-trivial solution is negative for $\alpha < 2.5906$. In the region $2.3336 < \alpha < 2.5906$ the RS solution is therefore non-physical, because the energy density of this problem must be positive by definition. In the RS approximation we have found a paramagnetic phase for $\alpha < 2.3336$ and a glassy phase for $\alpha > 2.5906$. This prediction is not correct, both quantitatively and qualitatively. The values of α where the transitions appear are not in agreement with numerical simulations, and there is a non-physical region.

3.4. Instability of evanescent field in the paramagnetic region

Before going to the 1RSB approximation, let us concentrate in this section on the RS paramagnetic region $\alpha < 2.3336$, in order to analyse the distribution of the so-called evanescent fields [19]. In the paramagnetic phase at zero temperature all the cavity fields h_i are null, but considering the first-order correction in temperature one can write $h_i = T h_i'$.

In terms of expectation values of spin variables, an evanescent field is the only one that can give a finite magnetization in the zero-temperature limit: $m = \tanh(\beta h) \to \tanh(h')$. In contrast, in the 'strictly' zero-temperature formalism that we use to study ground state energy, variables are either frozen, $|m| = 1$, or paramagnetic, $m = 0$, and we disregard any detailed information concerning the fluctuations of the local magnetizations of the unfrozen variables. The global probability distribution of the local magnetizations could in principle be non-trivial, with some variable polarized (yet never frozen) in some preferential direction.

There are two equivalent ways of obtaining such information on the distribution of magnetizations. The first consists in writing the iterative cavity equations for such magnetizations and then taking the average over the underlying random hypergraph. The second simply consists in computing the RS cavity equations at finite temperature assuming appropriate scaling of the cavity fields. Taking $h_i = T h_i'$ with h_i' finite leads, in the $\beta \to \infty$ limit, to a distribution of evanescent fields which may describe non-trivial expectations for the spins.

Following the same steps which brought us to the RS self-consistency equations (4), we can write analogously the self-consistency equations for the distributions of $h_i' = \beta h_i$ and

$u'_i = \beta u_i$ in the $\beta \to \infty$ limit. These equations look identical to those in equations (4), the only difference being the definition of the function $\hat{u}(h_1, h_2)$, which now reads

$$\hat{u}'(h'_1, h'_2) = \frac{\tanh(h'_1) + \tanh(h'_2)}{\tanh(h'_1)\tanh(h'_2) - 3}. \tag{11}$$

For very low α the only solution to the self-consistency equations is $P(h') = \delta(h')$. At variance with respect to other problems such as for instance 3-SAT [18] in which the low α phase is highly non-trivial, the bicolouring problem is simple. As happens in the Q-colouring [5] and in the three-spin problems [4, 17], the very low α phase is a genuine paramagnet, with local fields concentrated around zero even at the first order in temperature.

However, the solutions $P(h') = \delta(h')$ and $Q(u') = \delta(u')$ may become unstable at a certain value of α, which we call α_s. In order to study the stability of this solution (in which local fields are uncorrelated independent of the local structure of the underlying hypergraph) it is enough to give an infinitesimal width to $P(h')$ and check whether it increases or decreases under the iteration of equations (4). For very small values of h'_i one can linearize the function $\hat{u}'(h'_1, h'_2) \simeq -(h'_1 + h'_2)/3$ and obtain very simple relations among the variances of $P(h')$ and $Q(u')$ at two consecutive iterations (n and $n+1$):

$$\langle (u')^2 \rangle_{n+1} = \tfrac{2}{9} \langle (h')^2 \rangle_n \tag{12}$$

$$\langle (h')^2 \rangle_{n+1} = 3\alpha \langle (u')^2 \rangle_n. \tag{13}$$

For $\alpha < \alpha_s = 3/2$ the variances do not increase under iteration of the RS equations and the system is in a truly paramagnetic phase with all the magnetization identically zero.

For $\alpha > \alpha_s$, the presence of a broad distribution of first-order corrections h' suggests the presence of a full RSB spin-glass phase at finite temperature, produced by a 'replicon' instability at α_s. The finite-temperature phase transition at α_s corresponds at $T = 0$ to the onset of a non-trivial organization of ground states, with non-trivial magnetizations (unfrozen RSB scenario). We incidentally note that the value of α_s coincides with the best lower bound available for α_c.

However, as soon as the dynamical transition is reached at $\alpha_d \simeq 1.915$ (see the following section), the system loses memory of the unfrozen RSB phase. The non-evanescent fields, $h = \mathcal{O}(1)$, are the only ones relevant in determining the ground state energy. At the level of non-vanishing fields, at α_d we have a transition from RS to 1RSB. At this point, the analytically disconnected solution with vanishing fields disappears. The presence of full RSB is somehow accidental and we expect higher number of colours to disappear completely (as happens in graph colouring [5]).

4. The cavity 1RSB solution

4.1. Self-consistency equations: the distribution $\rho(\eta)$

In the previous section we have seen that the RS approximation produces a wrong solution. Here we study the system with a better approximation, the so-called one-step replica symmetry breaking.

In this approximation the scenario is a bit more complex: at α_d ($<\alpha_c$) there is a clustering phenomenon so that the computation made in the RS case is only valid within each state (cluster). The crossing between the energy of two states must be also considered, for which we use the 'reweighting parameter' μ as in [15].

The 1RSB order parameter is a distribution of distributions, whose self-consistency equations are as follows:

$$\mathcal{Q}[Q] = \int \mathrm{D}\mathcal{P}[P_1]\,\mathrm{D}\mathcal{P}[P_2]\,\delta^{(F)}\left[Q(u) - \int \mathrm{d}P_1(h_1)\,\mathrm{d}P_2(h_2)\,\delta(u - \hat{u}(h_1, h_2))\right] \tag{14}$$

$$\mathcal{P}[P] = \sum_{k=0}^{\infty} f_{3\alpha}(k) \int \prod_{i=1}^{k} \mathrm{D}\mathcal{Q}[Q_i] \times \delta^{(F)}\left[P(h) - \frac{1}{A_k}\int \prod_{i=1}^{k} \mathrm{d}Q_i(u_i)\,\mathrm{e}^{-\mu(\sum|u| - |\sum u|)}\,\delta\left(h - \sum_{i=1}^{k} u_i\right)\right] \tag{15}$$

with $\delta^{(F)}$ being a functional delta and A_k normalization coefficients.

Thanks to the system symmetries, the most general form for $Q(u)$ is given by

$$Q(u) = \eta\delta(u) + \frac{1-\eta}{2}[\delta(u+1) + \delta(u-1)] \tag{16}$$

which is symmetric under $u \leftrightarrow -u$ and with $u \in \{-1, 0, 1\}$. The heterogeneity of the random hypergraphs is now reflected in the very different values η may take: for example, isolated plaquettes certainly have $\eta = 1$. Let us call $\rho(\eta)$ the probability distribution function of η. The problem will be now studied in terms of $\rho(\eta)$, which completely determines the order parameter $\mathcal{Q}[Q]$.

4.2. $\mu \to \infty$ limit

Self-consistency equations (14) and (15) can be written as a single self-consistency equation for the distribution $\rho(\eta)$. In the $\mu \to \infty$ limit it reads

$$\rho(\eta) = \sum_{k=0}^{\infty} f_{3\alpha}(k) \sum_{k'=0}^{\infty} f_{3\alpha}(k') \int \prod_{i=1}^{k} \mathrm{d}\rho(\eta_i) \prod_{j=1}^{k'} \mathrm{d}\rho(\eta'_j) \times \delta\left[\eta - 1 + \frac{1}{2}\left(1 - \frac{\prod_{i=1}^{k}\eta_i}{A_k}\right)\left(1 - \frac{\prod_{j=1}^{k'}\eta'_j}{A_{k'}}\right)\right] \tag{17}$$

with the normalization coefficients $A_k = 2\prod_{i=1}^{k}\frac{1+\eta_i}{2} - \prod_{i=1}^{k}\eta_i$. Equation (17) can be solved by a population dynamics algorithm. Starting from a population of η randomly distributed in $[0, 1]$ we then iterate the following steps:

- take k elements and compute η^k and A_k, where k, is a Poissonian number;
- take k' elements and compute $\eta^{k'}$ and $A_{k'}$, where k' also is a Poissonian number;
- compute a new η as

$$1 - \frac{1}{2}\left(1 - \frac{\eta^k}{A_k}\right)\left(1 - \frac{\eta^{k'}}{A_{k'}}\right)$$

  and insert it in the population eliminating another random η.

The asymptotic distribution $\rho(\eta)$ is plotted in figure 3 (left) for different values of α. For $\alpha > \alpha_d \simeq 1.915$ the distribution has both a trivial contribution in 1 and a non-trivial one in the $\left[\frac{1}{2}; 1\right]$ region, while for $\alpha < \alpha_d$ it collapses into a single delta function in 1.

In figure 3 (right) we plot the average value of η versus α, by which we immediately localize the dynamical phase transition at $\alpha_d = 1.915$. An identical curve has been calculated analytically in the more tractable case of the p-spin model [4].

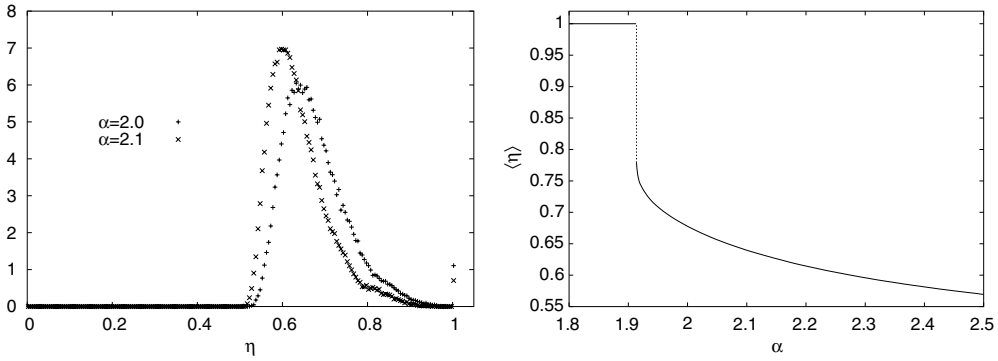

Figure 3. Left: probability distribution $\rho(\eta)$ for $\alpha = 2.0$ and $\alpha = 2.1$. Note the trivial contribution in 1. Right: average value of η versus α. This value is exactly 1 for $\alpha < \alpha_d = 1.915$.

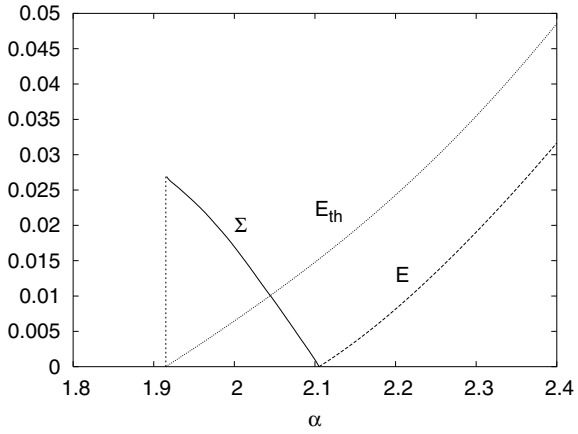

Figure 4. Phase diagram of random hypergraph bicolouring.

4.3. Complexity

In the $\mu \to \infty$ limit the complexity is given by [15]

$$\Sigma = \lim_{\mu\to\infty}(-\mu\Phi) = \lim_{\mu\to\infty}\left\{\overline{\log A_k} - 2\alpha\,\overline{\log\left[1 - \frac{1}{2}(1-\eta)\left(1 - \frac{\eta^k}{A_k}\right)\right]}\right\} \tag{18}$$

where the averages are taken with respect to the Poissonian distribution of k and with respect to $\rho(\eta)$.

The complexity curve is plotted in figure 4. We identify the critical point $\alpha_c = 2.105$, which corresponds to the SAT/UNSAT transition, as the point where the complexity vanishes.

4.4. Energy density and 1RSB phase diagram

In order to evaluate free energy Φ we must generalize the computation for finite values of μ.

The self-consistency equation for general μ is

$$\rho(\eta) = \sum_{k=0}^{\infty} f_{3\alpha}(k) \sum_{k'=0}^{\infty} f_{3\alpha}(k') \int \prod_{i=1}^{k} \mathrm{d}\rho(\eta_i) \prod_{j=1}^{k'} \mathrm{d}\rho(\eta'_j) \delta \left[\eta - 1 + \frac{1}{2} \left(1 - \frac{a_k}{A_k}\right) \left(1 - \frac{a_{k'}}{A_{k'}}\right) \right] \tag{19}$$

where a_k is the coefficient of the delta function in 0 of the distribution $P^{(k)}(h)$ computed by the convolution of k biases u, and A_k is its normalization factor. To compute quickly the $P^{(k)}(h)$ we can use a recursive relation:

$$P^{(k)}(h) = \int \mathrm{d}Q_k(u_k)\, \mathrm{d}P^{(k-1)}(g) \delta(h - g - u_k)\, \mathrm{e}^{-\mu(|u_k|+|g|-|g+u_k|)}. \tag{20}$$

The free energy is given by $\Phi = \Phi_1 - 2\alpha\Phi_2$ with

$$\begin{aligned} \Phi_1 &= -\frac{1}{\mu} \overline{\log(A_k)} \\ \Phi_2 &= -\frac{1}{\mu} \overline{\log\left(1 - \frac{1}{2}(1-\eta)\left(1 - \frac{a_k}{A_k}\right)(1 - \mathrm{e}^{-2\mu})\right)}. \end{aligned} \tag{21}$$

For $\alpha > \alpha_c$, Φ has a maximum at a finite value of μ, which means that the ground state has positive energy. Otherwise for $\alpha < \alpha_c$, Φ is always negative, converging towards zero for $\mu \to \infty$, which corresponds to a zero-energy ground state.

The energy density is calculated as

$$E = \frac{\partial}{\partial\mu}(\mu\Phi) = -\frac{1}{A_k}\frac{\partial A_k}{\partial\mu} + 2\alpha \frac{(1-\eta)\left(1 - \frac{a_k}{A_k}\right)\mathrm{e}^{-2\mu}}{1 - \frac{1}{2}(1-\eta)\left(1 - \frac{a_k}{A_k}\right)(1 - \mathrm{e}^{-2\mu})}. \tag{22}$$

As we did before, rather than computing the derivative of the A_k, we can write a recursive equation for the probability distribution $R^{(k)}(h) \equiv \frac{\partial}{\partial\mu} P^{(k)}(h)$:

$$\begin{aligned} R^{(k)}(h) = \int \mathrm{d}Q_k(u_k)\, \mathrm{d}g [& R^{(k-1)}(g) \\ & + (|h| - |g| - |u_k|) P^{(k-1)}(g)] \delta(h - g - u_k)\, \mathrm{e}^{-\mu(|g|+|u_k|-|h|)}. \end{aligned} \tag{23}$$

Including this calculation in the population dynamics algorithm provides directly the curve $E(\mu) = \frac{\partial}{\partial\mu}(\mu\Phi)$. The ground state energy is obtained as the point where $E(\mu)$ and $\Phi(\mu)$ coincide.

The ground state energy density is compared to the numerical results in figure 5. This curve must be considered an $N \to \infty$ limit of the finite N curves that we obtained numerically.

Another interesting curve that we can compute is the complexity versus the energy, which we plot parametrically in μ using $E(\mu)$ and $\Phi(\mu)$ (see figure 6). The curve $\Sigma = \mu(E - \Phi)$ has two branches: the lower one is the physical one and represents the true complexity[5].

The last quantity we display in figure 4 is E_{th} versus α, which is simply the maximum of $E(\mu)$.

Summarizing the 1RSB results we get the following scenario.

There is a 'paramagnetic' phase for $\alpha < \alpha_d = 1.915$, where there are no metastable states and we conjecture the existence of linear algorithms for colouring the generic hypergraph. The cavity fields are zero, so the spins are not forced to be black or white. In the so-called HARD-SAT region $\alpha_d < \alpha < \alpha_c = 2.105$ the generic hypergraph is still colourable, but the

[5] For the unphysical one there is not still a precise interpretation [15], however it does not seem to have any physical meaning.

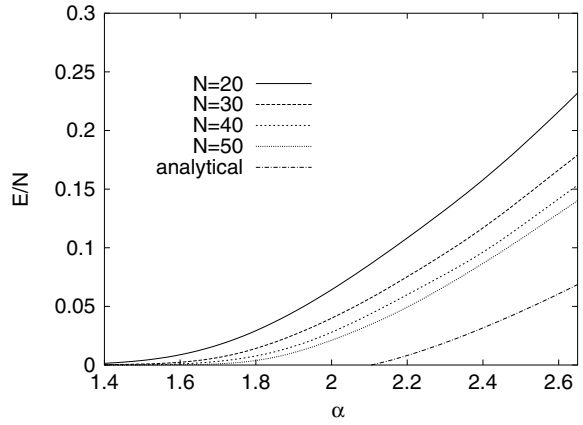

Figure 5. Energy density of random hypergraph bicolouring: comparison among finite-size numerical results and analytical 1RSB solution.

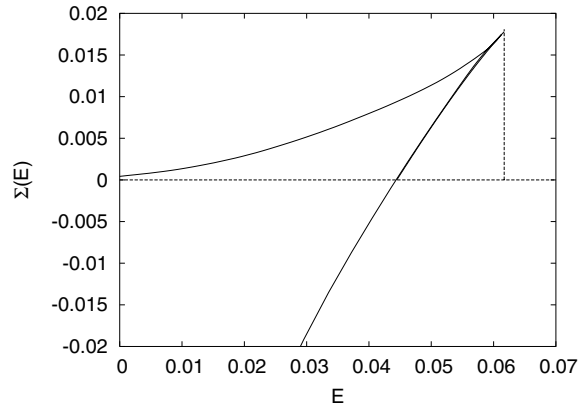

Figure 6. Complexity versus energy at $\alpha = 2.5$: note the non-physical upper branch. Along the physical lower branch at the threshold energy $E_{\rm th} = 0.062$ the complexity is maximal, while it becomes zero at the ground state energy.

presence of many states makes the colouring procedure very difficult. In each ground state there is a core of spins for which there is a particular pattern of colouring: because of the existence of an exponentially larger number of metastable states, it is very difficult for the local search algorithm to colour the core in the right way. For $\alpha > \alpha_d$ the 1RSB approximation becomes less valid when high energy states are considered [20]. Most likely, the curve $E_{\rm th}$ would slightly change if a better approximation is used.

These 1RSB results are expected to be a very good approximation of the exact analytical solution, as happens in the majority of similar combinatorial optimization problems. For the p-spin model [17] an exact solution has been found that is identical to the 1RSB one [4, 21].

5. Single-sample analysis and the SP algorithm

An innovative and useful reformulation of the cavity equations has been proposed in [7]. The self-consistency equations are used to study single random problem instances and allow us to

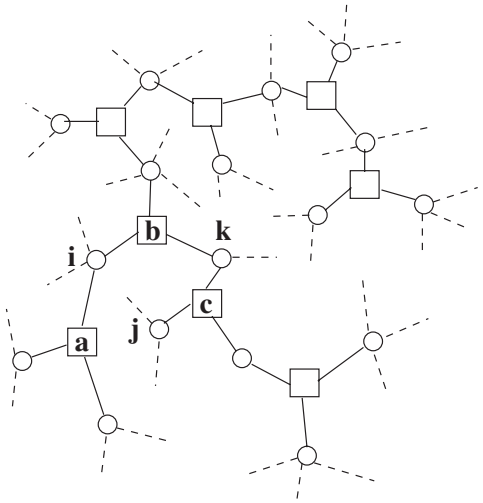

Figure 7. Factor graph representation of an energy minimization problem.

get microscopic information about the behaviour of the single spins in the stable and metastable states of given energy density. The method, called survey propagation (SP), is general and provides the core ingredient of a new efficient algorithm [3, 7, 22] for finding ground states within the glassy phase. Here we will apply and check SP for the bicolouring problem. This problem is half-way between the random K-SAT problem and the random K-XORSAT (or p-spin) problem. Since the SP algorithm does work for random K-SAT [7], but it does not seem to work for random K-XORSAT, we believe that it is of primary importance to check its performances on the random hypergraph bicolouring problem.

The iterative equations for the probability distributions of cavity fields that we have used in the previous sections to find the phase diagram were implemented at the same time during a population dynamics process and an averaging over the random realizations. However, the equations can be easily iterated over specific realizations, that is avoiding the averaging step. In such a formulation the order parameter becomes the full list of the cavity fields over the entire graph. From the cavity fields one may determine the bias of each spin in all metastable states of given energy density and this information can be used for algorithmic purposes. The underlying hypothesis for the exactness of the single-sample formalism is the validity of the so-called clustering condition within states: cavity fields should be uncorrelated within states and we expect this to be approximatively true, thanks to the fact that the most numerous loops in the graph have a length that diverges as $\log N$.

In order to set up an appropriate formalism for the single-sample analysis, we resort to the factor graph representation [23] of the bicolouring problem: variables are represented by N circular 'variable nodes' labelled with letters $i, j, k, \ldots$ whereas links (which carry the interaction energy) are represented by M square 'function nodes' labelled by $a, b, c, \ldots$ (see figure 7). Function nodes have connectivity 3, variable nodes have a Poisson connectivity of average 3α and the overall graph is bipartite. The energy function can be trivially written as the sum over function nodes of their energies.

Following [7], we call 'messages' the $\hat{u}$ terms which represent the contribution to the cavity fields coming from the different connected branches of the graph. In the message-passing language (typical of error-correcting code algorithms [24]) one may describe the SP

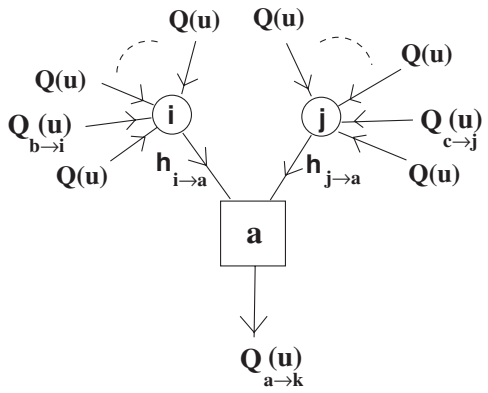

Figure 8. Iterative equations as message-passing procedure.

equations as follows. In the replica symmetric approximation, the messages arriving at a node are added up and then sent to a function node. Next, the function node transforms all input signals into a new message which is sent to the descendant variable node. At the 1RSB level, the messages along the links of the factor graph are u-surveys of usual messages over the various possible states of the system at a given value of the energy (which is fixed by the reweighting parameter μ). While the method is not restricted to zero temperature, at $T = 0$ it assumes a particularly simple form because messages can take only few values, 3 in our case, and the u-surveys are given by the probabilities of these values. The u-surveys are parametrized by two real numbers and the SP can be implemented easily. Each edge $a \to j$ from a function node to a variable node j carries a u-survey $Q_{a\to j}(u)$. The algorithm finds these u-surveys and all the cavity fields $P_{i\to a}(h)$. Very schematically, the procedure works as follows. All the u-surveys $Q_{a\to i}(u)$ are initialized randomly. Next, function nodes are selected sequentially at random and the u-surveys are updated according to the following equations:

$$P_{i\to a}(h) = C_{i\to a}\int \mathrm{d}u_1 \cdots \mathrm{d}u_k\, Q_{b_1\to i}(u_1)\cdots Q_{b_k\to i}(u_k)\delta \times \left(h - \sum_{a=1}^{k} u_a\right)\exp\left(\mu\left(\left|\sum_{a=1}^{k} u_a\right| - \sum_{a=1}^{k}|u_a|\right)\right) \tag{24}$$

$$Q_{a\to i}(u) = C_{a\to i}\int \mathrm{d}g\,\mathrm{d}h\, P_{j\to a}(g)P_{\ell\to a}(h)\delta(u - \hat{u}_(g,h)) \tag{25}$$

where the function $\hat{u}(g,h)$ is that defined in equation (3). In the above expressions, $C_{i\to a}$, $C_{a\to i}$ are normalization constants and the labels b_i identify the k neighbouring function nodes different from a connected to site the variable node i (see figure 8).

Parametrizing the u-surveys as

$$Q_{a\to i}(u) = \left(1 - \eta^{+}_{a\to i} - \eta^{-}_{a\to i}\right)\delta(u) + \eta^{+}_{a\to i}\delta(u-1) + \eta^{-}_{a\to i}\delta(u+1) \tag{26}$$

the above set of equations (24), (25) defines a nonlinear map over the η.[6]

[6] In the algorithmic formalism we need a more general parametrization of surveys with respect to that used in the first sections. As we shall see, along the decimation process the symmetries of surveys are lost.

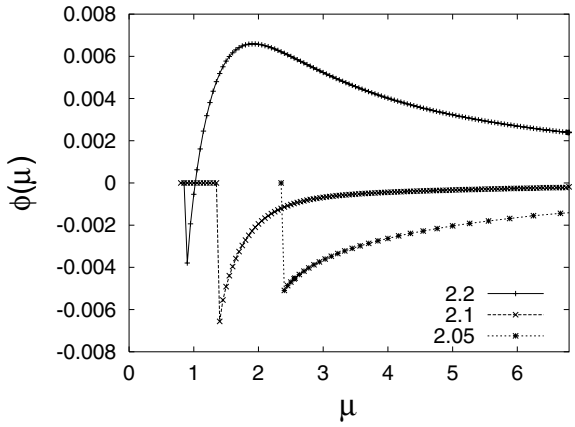

Figure 9. Free energy $\phi(\mu)$ for different samples of size $N = 10\,000$ and $\alpha = 2.05, 2.1, 2.2$.

The process is iterated until convergence is reached and finally the stable set of u-surveys is used to compute the N local field $\{P_i(H_i)\}$ distributions and the free energy $\Phi(\mu)$. We have

$$P_i(H) = C_i \int \prod_{a\in V(i)} \mathrm{d}u_a Q_{a\to i}(u_a)\delta\left(H - \sum_{a\in V(i)} u_a\right) \exp\left(\mu\left(\left|\sum_{a\in V(i)} u_a\right| - \sum_{a\in V(i)} |u_a|\right)\right) \tag{27}$$

with C_i being the normalization constant and $V(i)$ the set of function nodes connected to variable i. The free energy reads

$$\Phi(\mu) = \frac{1}{N}\left(\sum_{a=1}^{M} \Phi_a^f(\mu) - \sum_{i=1}^{N} \Phi_i^v(\mu)(n_i - 1)\right) \tag{28}$$

where

$$\begin{aligned}
\Phi_a^f(\mu) &= -\frac{1}{\mu}\log\left\{\int \prod_{i\in V(a)}\left[\prod_{b\in V(i)-a} Q_{b\to i}(u_{b\to i})\,\mathrm{d}u_{b\to i}\right]\right. \\
&\qquad \left.\times \exp\left[-\mu \min_{\{\sigma_i, i\in V(a)\}}\left(E_a - \sum_{i\in V(a)}\left[\sum_{b\in V(i)-a} u_{b\to i}\right]\sigma_i + \sum_{b\in V(i)-a}|u_{b\to i}|\right)\right]\right\} \\
\Phi_i^v(\mu) &= -\frac{1}{\mu}\log\left\{\int \prod_{a\in V(i)} \mathrm{d}u_a\, Q_{a\to i}(u_a)\exp\left[\mu\left(\left|\sum_{a\in V(i)} u_a\right| - \sum_{a\in V(i)}|u_a|\right)\right]\right\} \\
&= -\frac{1}{\mu}\log(C_i).
\end{aligned} \tag{29}$$

In the above expressions, $V(a)$ identifies the set of variable nodes connected to the function node a and E_a is its energy (i.e. the link energy).

The complexity $\Sigma(\mu) = \partial\Phi(\mu)/\partial(1/\mu)$ and the energy density $\epsilon(\mu) = \partial(\mu\Phi(\mu))/\partial\mu$ of states can also be estimated over single instances. Figure 9 shows the free energy $\phi(\mu)$ of

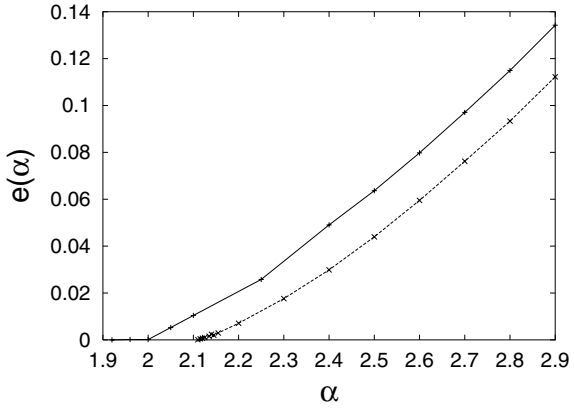

Figure 10. Ground state energy and threshold energy for a single sample of size $N = 10\,000$ at different connectivities.

single graphs with $N = 10\,000$ vertices as a function of μ for different values of the average connectivity α. Figure 10 shows the ground state energies and threshold energies for single instances at different α. Similar data can be produced for the complexity. The agreement with the averaged calculations of the previous sections is indeed remarkable already for relatively small values of N (as should be expected from the self-averaging property of the free energy).

Once the information concerning the effective local fields acting on the single spin variables becomes available a decimation procedure for finding ground states can be easily implemented. We have done one such implementation for the $\mu \to \infty$ case, with the scope of finding perfect colourings in the dynamical region just below α_c. In this regime, the expression of the nonlinear map simplifies considerably. From equations (24), (25) we find

$$\begin{aligned} \eta^{+}_{a\to i} &= \prod_{j\in V(a)\setminus i}\left[\frac{\Pi^{-}_{j\to a}}{\Pi^{0}_{j\to a}+\Pi^{-}_{j\to a}+\Pi^{0}_{j\to a}}\right] \\ \eta^{-}_{a\to i} &= \prod_{j\in V(a)\setminus i}\left[\frac{\Pi^{+}_{j\to a}}{\Pi^{+}_{j\to a}+\Pi^{-}_{j\to a}+\Pi^{0}_{j\to a}}\right] \end{aligned} \tag{30}$$

where

$$\begin{aligned} \Pi^{+}_{j\to a} &= \prod_{b\in V(j)\setminus a}(1-\eta^{-}_{b\to i}) - \prod_{b\in V(j)\setminus a}\eta^{0}_{b\to i} \\ \Pi^{-}_{j\to a} &= \prod_{b\in V(j)\setminus a}\left(1-\eta^{+}_{b\to i}\right) - \prod_{b\in V(j)\setminus a}\eta^{0}_{b\to i} \\ \Pi^{0}_{j\to a} &= \prod_{b\in V(j)\setminus a}\eta^{0}_{b\to i}. \end{aligned} \tag{31}$$

The value of $\eta^{0}_{a\to j}$ can be calculated by normalization. Other relevant quantities such as the biases of variables and the complexity also acquire a simple form. Upon defining the bias $W_i^{\pm,0}$ of a variable as the probability of picking up a cluster of ground states at random and finding that variable frozen in some preferential direction, that is $W_i^{+} \equiv \mathrm{Prob}(H_i > 0)$, $W_i^{0} \equiv \mathrm{Prob}(H_i = 0)$, $W_i^{-} \equiv \mathrm{Prob}(H_i < 0)$, we have

$$
\begin{aligned}
W_i^+ &= \frac{\hat{\Pi}_i^+}{\hat{\Pi}_i^+ + \hat{\Pi}_i^- + \hat{\Pi}_i^0} \\
W_i^- &= \frac{\hat{\Pi}_i^-}{\hat{\Pi}_i^+ + \hat{\Pi}_i^- + \hat{\Pi}_i^0} \\
W_i^0 &= 1 - W_i^{(+)} - W_i^{(-)}
\end{aligned}
\tag{32}
$$

with

$$
\begin{aligned}
\hat{\Pi}_i^+ &= \prod_{a \in V(i)} (1 - \eta_{a\to i}^-) - \prod_a \eta_{a\to i}^0 \\
\hat{\Pi}_i^- &= \prod_{a \in V(i)} \left(1 - \eta_{a\to i}^+\right) - \prod_a \eta_{a\to i}^0 \\
\hat{\Pi}_i^0 &= \prod_{a \in V(i)} \eta_{a\to i}^0
\end{aligned}
\tag{33}
$$

For the complexity we have

$$
\Sigma = \frac{1}{N}\left(\sum_{a=1}^{M} \Sigma_a - \sum_{i=1}^{N} (n_i - 1)\Sigma_i\right) \tag{34}
$$

where

$$
\Sigma_a = \log\left[\prod_{j \in V(a)} \left(\Pi_{j\to a}^+ + \Pi_{j\to a}^- + \Pi_{j\to a}^0\right) - \prod_{j \in V(a)} \Pi_{j\to a}^+ - \prod_{j \in V(a)} \Pi_{j\to a}^-\right] \tag{35}
$$

$$
\Sigma_i = \log\left[\hat{\Pi}_i^+ + \hat{\Pi}_i^- + \hat{\Pi}_i^0\right]. \tag{36}
$$

With the list of the biases in hand, the following simple decimation procedure for finding ground state configurations can been implemented:

1. $\{\eta\} \leftarrow$ `random`
2. `SP`
   (a) `Iterate equations` (24), (25) `until a fixed` $\{\eta^*\}$ `point is reached`
3. `Compute the biases` $W_i^+ = \mathtt{Prob}(H_i > 0)$, $W_i^0 = \mathtt{Prob}(H_i = 0)$, $W_i^- = \mathtt{Prob}(H_i < 0)$, `following equation` (27)
4. `For` $B_i = W_i^+ - W_i^-$, `choose` i `such that` $|B_i|$ `is maximum`
5. `IF` $|B_i| < \epsilon$ `for all` i `then STOP (paramagnetic state) and output the reduced sub-problem`
6. `FIX` $\sigma_i = 1$ `if` $B_i > 0$, $\sigma_i = -1$ `otherwise`
7. `GOTO 2`

One should note that along the decimation procedure some of the variables are fixed and therefore new types of links appear. The corresponding new function nodes will have an energy which is inherited by the three-body interaction by fixing one of the variables. Once decimation has started, the bicolouring problem becomes a mixture of graph and hypergraph bicolouring.

The behaviour of the algorithm on sufficiently large ($n > 10^3$) random bicolouring instances is as follows:

- For low α ($\alpha < \alpha_d$), the variables turn out to be all paramagnetic (zero bias).
- In the dynamical region the biases are non-trivial and the decimation procedure fixes many variables leading to sub-problems which are paramagnetic and easily solved by a greedy heuristic. Very close to α_c the decimation procedure may fail in finding solutions in the first run. In this region the algorithm can be improved in many ways, e.g., by a random restart or a backtrack or a different decimation strategy. In any case we cannot exclude the existence of a threshold close to α_c where the decimation procedure stops converging.

For small N the structural 'rare events' of the random hypergraph, such as links sharing more than one variable or other types of short loops, require an appropriate (in principle simple) modification of the SP iterations [24]. More in general, the presence of loops of different length scales may introduce correlations which may require further non-trivial generalization of the whole SP procedure.

6. Conclusions

In this work we have given a very detailed description of the random hypergraph bicolouring problem, both in the average case and in single samples.

After having defined the statistical model corresponding to this problem, we have applied the cavity method to solve it: results in the RS and 1RSB approximations have been presented.

Increasing the connectivity α the model undergoes several phase transitions, which can be summarized as follows:

- For $\alpha < \alpha_s$ the model is in a genuine paramagnetic phase; all the magnetizations are identically null.
- At $\alpha = \alpha_s$ a 'replicon' instability takes place, which manifests at finite temperature with the onset of spin-glass order (full RSB).
- For $\alpha_s < \alpha < \alpha_d$ the presence of a full RSB phase at finite temperatures is reflected in the ground states by finite values for the spin magnetizations.
- At $\alpha = \alpha_d$ a clustering transition takes place among the ground states. They split in an exponentially large number of clusters. Within each cluster a finite fraction of variables are completely frozen (backbone).
- For $\alpha_d < \alpha < \alpha_c$ the model has a nonzero complexity and an exponentially large number of metastable states, which may block local search algorithms. Although there are very strong correlations among variables the ground state energy is still zero and the problem is colourable on average.
- At $\alpha = \alpha_c$ the COL/UNCOL phase transition takes place.
- For $\alpha > \alpha_c$ the ground state energy is positive and the problem cannot be coloured on average.

In the second part of this work we have applied the survey propagation algorithm to problem instances taken from the HARD-COL region ($\alpha_d < \alpha < \alpha_c$), finding in polynomial time solutions to the problem. So we have verified that the SP algorithm works properly also for this model, which is more difficult than the 3-SAT problem [7]. Indeed this model, at variance with K-SAT, has no local biases which could in principle be exploited by a smart algorithm.

Next steps in this line of research will be to consider random difficult combinatorial problems endowed with some non-trivial local structure of the underlying graph. This constitutes a conceptual challenge that will bring the algorithmic and analytical tools developed for sparse graphs closer to what is found in the real-world version of the same class of models [25].

References

[1] Karp R 1972 *Complexity of Computer Computation* ed E Miller and J W Thatcher (New York: Plenum) p 85
[2] Friedgut E 1999 *J. Am. Math. Soc.* **12** 1017
[3] Mézard M, Parisi G and Zecchina R 2002 *Science* **297** 812
[4] Mézard M, Ricci-Tersenghi F and Zecchina R 2003 *J. Stat. Phys.* **111** 505
[5] Braunstein A, Mulet R, Pagnani A, Weigt M and Zecchina R 2003 *Preprint* cond-mat/0304558 (*Phys. Rev.* E at press)
[6] Braunstein A, Leone M, Ricci-Tersenghi F and Zecchina R 2002 *J. Phys. A: Math. Gen.* A **35** 7559
[7] Mézard M and Zecchina R 2002 *Phys. Rev.* E **66** 056126
[8] Alon N and Spencer J A note on coloring random k-sets (unpublished manuscript)
[9] Achlioptas D and Moore C 2002 *Proc. RANDOM 02*
[10] Achlioptas D, Han Kim J, Krivelevich M and Tetali P 2002 *Random Struct. Algorithms* **20** 249
[11] Guerra F and Toninelli F L 2002 *Commun. Math. Phys.* **230** 71
Guerra F 2002 *Preprint* cond-mat/0205123
[12] Franz S and Leone M 2003 *J. Stat. Phys.* **111** 535
[13] Hayes B 1997 *Am. Sci.* **85** 2
[14] Mézard M and Parisi G 2001 *Eur. Phys. J.* B **20** 217
[15] Mézard M and Parisi G 2003 *J. Stat. Phys.* **111** 1
[16] van Mourik J and Saad D 2002 *Phys. Rev.* E **66** 056120
[17] Ricci-Tersenghi F, Weigt M and Zecchina R 2001 *Phys. Rev.* E **63** 026702
[18] Monasson R and Zecchina R 1997 *Phys. Rev.* E **56** 1357
[19] Biroli G, Monasson R and Weigt M 2000 *Eur. Phys. J.* B **14** 551
[20] Montanari A and Ricci-Tersenghi F 2003 *Eur. Phys. J.* B **33** 339
[21] Cocco S, Dubois O, Mandler J and Monasson R 2003 *Phys. Rev. Lett.* **90** 047205
[22] Braunstein A, Mézard M and Zecchina R 2002 *Preprint* org/cs.CC/0212002
[23] Kschischang F R, Frey B J and Loeliger H-A 2002 *IEEE Trans. Inf. Theory* **47** 498
[24] Yedida J S, Freeman W T and Weiss Y 2001 *Advances in Neural Processing Systems* vol 13, ed T K Leen, T G Dietterich and V Tresp (Cambridge, MA: MIT Press) pp 689–95
[25] www.satlib.com